The Multi-Filter Rotating Shadowband Radiometer (MFRSR) - Precision Infrared Radiometer (PIR) Platform in Fairbanks: Scientific Objectives

K. Stamnes and E. Leontieva
Geophysical Institute
University of Alaska Fairbanks
Fairbanks, Alaska

Arctic Qualification of the Multi-Filter Rotating Shadow-band Radiometer (MFRSR) and Precision Infrared Radiometer (PIR) Instruments

The MFRSR and the PIR have been deployed at the Geophysical Institute in Fairbanks to check their performance under arctic conditions. Drawing on the experience of the previous measurements in the Arctic, the PIR was equipped with a ventilator to prevent the build-up of frost and moisture on the its dome.

We adopted the Solar Infrared (IR) Observing System (SIROS) concept from the Southern Great Plains Atmospheric Radiation Measurement Site to allow implementation of the same data processing software for a set of radiation and meteorological instruments.

The ongoing work is focused on practical problems and is in the stage of testing the sensors and data acquisition system.

To validate the level of performance of the whole SIROS prior to its incorporation into the North Slope of Alaska (NSA) Cloud and Radiation Testbed Site instrumental suite for flux radiation measurements, the comparison between measurements and model predictions will be undertaken to assess the MFRSR - PIR Arctic data quality.

Potential for Determining Cloud Properties from MFRSR Data

A preliminary feasibility study of the MFRSR capabilities in conjunction with comprehensive radiative transfer computations to infer cloud optical properties was performed (Leontieva and Stamnes 1994). We assume that the surface albedo is known from the measurements of a MFRSR unit that operates without a shadowband looking down.

We propose to consider transmittances rather than irradiances because this allows us to deal only with the uncalibrated outputs of the instrument and makes the precision to which the filter functions are needed to be known less critical. The use of transmittances is highly beneficial from the computational point of view since an efficient algorithm is available to compute the transmittance for the earth-atmosphere system including vertical atmospheric inhomogeneity (Stamnes 1982). Figure 1 shows the look-up tables of computed transmittances for a specific day at Barrow, Alaska, having a step of 0.005 over cos(SZA). Figure 1 demonstrates the possible effect of aerosol extinction on transmittance implying the usefulness of commonly observed atmospheric optical depths at a particular location that will be continuously retrieved from the MFRSR measurements of direct solar irradiance under true cloud-free conditions. The use of observational values of aerosol optical depths becomes especially desirable at high surface albedo.

Model simulations show that both cloud optical depth and cloud droplet effective radius could be inferred from the measurements of bispectral transmittance, using a combination of any wavelength without liquid water absorption (for example, 862 nm) and a 2250 nm wavelength. Two sets of contour curves presented in Figure 2 illustrate the possibility of simultaneously retrieving cloud optical depth and effective radius at least in the range of τ from 3 to 30. Better results are also anticipated at smaller, $r_e < 6$ μm, drop sizes.

A method for simultaneously retrieving both cloud optical depth and surface albedo from measurements of down welling spectral irradiances in the visible part of the spectrum has been introduced by Ricchiazzi et al. (1995). We

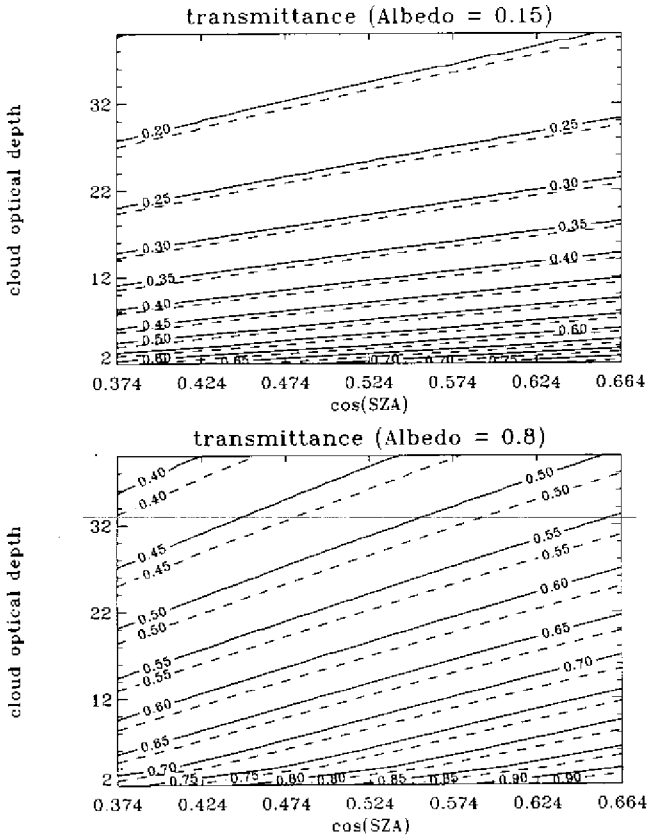

Figure 1. Contours of the computed transmittance at 862-nm MFRSR passband, for subarctic summer atmosphere and two aerosol models: MODTRAN h6 , atmosphere optical depth τ = 0.105 (solid lines) and the scaled model τ = 0.2 (dashed lines). The range of cos(SZA) corresponds to DAY=180, Barrow, Alaska (SZA < 70 deg.).

propose to test and apply this method to the measurements of transmittances in any pair of MFRSR channels (excluding 940 nm). Figure 3 provides a graphical illustration of the retrieval method and displays the contour plot of computed transmittances for two MFRSR channels, namely at 415-nm and 862-nm passbands.

Thermal IR Irradiance at the Surface: Model Predictions and Observations at Barrow, Alaska

The downward longwave irradiances measured by the PIR at the National Oceanic and Atmospheric Administration Climate Monitoring and Diagnostics Laboratory (CMDL) station at Barrow, Alaska, during 1988 and 1992 have

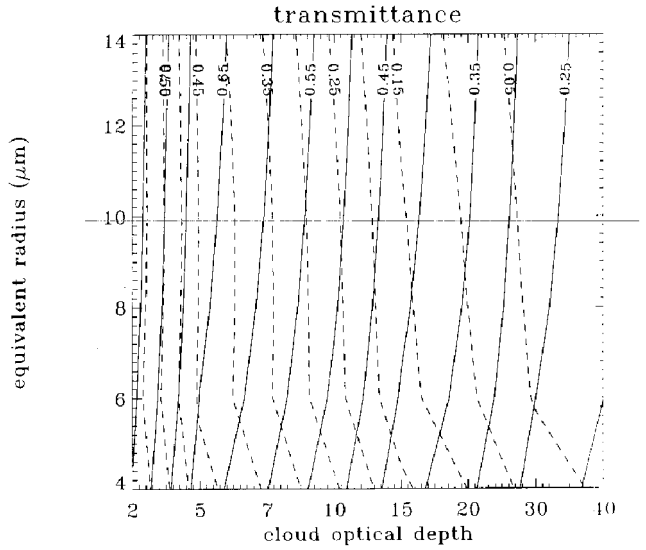

Figure 2. Contours of the computed transmittance at 862-nm MFRSR passband (solid lines), and at 2250 nm (dashed lines) for subarctic summer atmosphere and MODTRAN haze=6 tropospheric aerosol model at surface albedo A = 0.15. SZA = 45 deg.

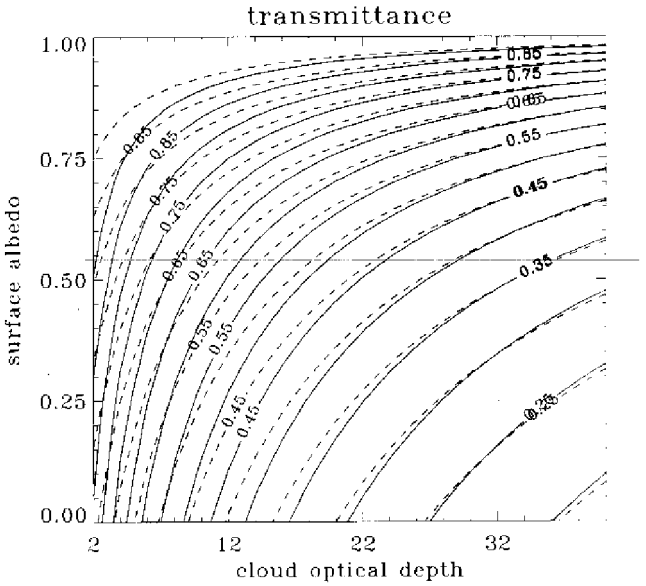

Figure 3. Contours of the computed transmittance at 862 nm (solid lines) and at 415 nm (dashed lines) of the MFRSR for subarctic summer atmosphere and MODTRAN haze=6 tropospheric aerosol model. SZA = 45 deg.

been compared with the model estimations based on radiosonde sounding data. The analysis was restricted to the times reported to be cloud free. Scatterplots of

measured hourly-averaged IR fluxes at the surface versus calculated values are shown in Figure 4. The measurements made by the ventilated version of PIR in 1992 produce better agreement with the modeled values as compared with corresponding magnitudes in 1988 (PIR without ventilator). Table 1 presents the linear regression results for both data sets.

Although a better agreement between measurements and computations in 1992 might also be caused by different atmospheric conditions, we believe that these results demonstrate an improved quality of the IR flux measurements by the modified PIR in the Arctic. Generally, measured "clear sky" downward IR flux in winter appeared to be greater than expected from the model predictions that by implication were associated with lower tropospheric ice crystals.

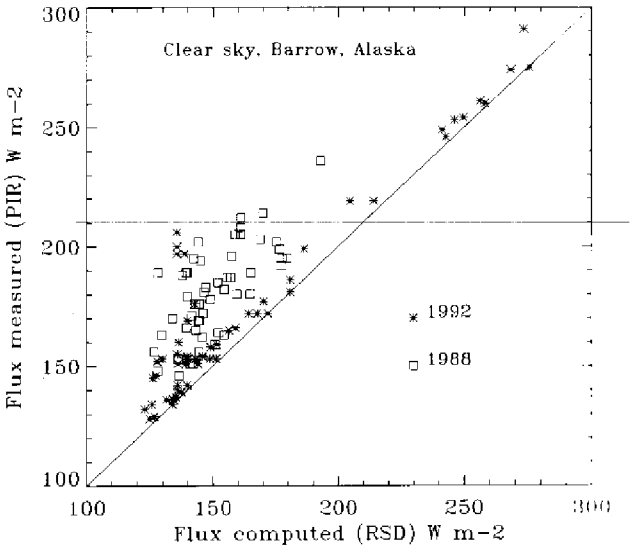

Figure 4. A scatterplot of measured versus computed downward IR irradiance at the surface.

The impact of ice crystals as compared to water droplets (fog) on the downward IR flux at the surface is shown in Figure 5 based on model simulations. The radiative properties of clouds were modeled in terms of particle effective size and ice (liquid) water content using parameterizations of Fu and Liou (1993) and Hu and Stamnes (1993) for ice and water cloud, respectively. An increase in effective particle size (both drops and ice crystals) causes a decrease in downwelling IR flux at the surface and an increase in outgoing IR flux to space since the clouds become less opaque. For the same effective size and water path, the ice cloud is more "black" as compared with water cloud.

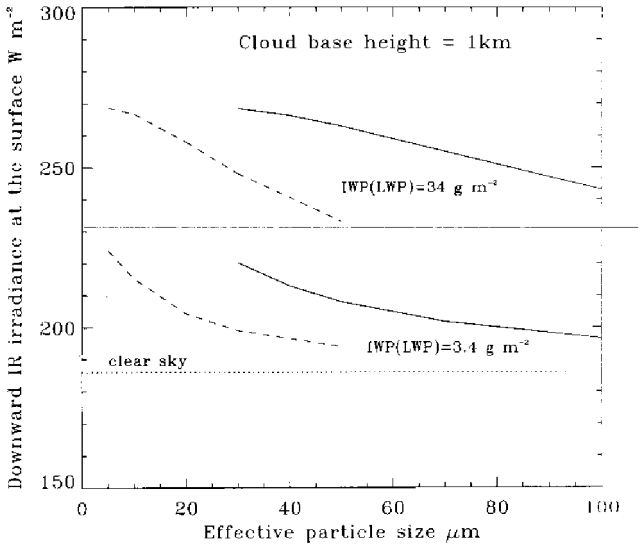

Figure 5. Downward IR irradiance at the surface versus effective cloud particle size (ice crystals shown as solid line; water droplets shown as dashed line).

Table 1. Comparison between measured and calculated downward longwave fluxes under clear skies.

Year	Number	Rms difference $W m^{-2}$	Bias (Meas-calc)	Slope	Intercept	Corr. Coeff.
1988	52	33	30	0.9	45	0.70
1992	55	20	13	0.9	29	0.94

References

Fu, Q., and K. N. Liou. 1993. Parameterization of the radiative properties of cirrus clouds, *J. Atmos. Sci.*, **50**(13), 2008-2025.

Hu, Y. X., and K. Stamnes. 1993. An accurate parameterization of the radiative properties of water clouds suitable for use in climate models, *J. Clim.*, **6**, 728-741.

Leontieva, E., and K. Stamnes. 1994. Remotely sensed measurements of cloud optical depth using a ground-based Multi-Filter Rotating Shadowband Radiometer in the Arctic (Methodology). In *3rd Circumpolar Symposium on Remote Sensing of Arcti c Environments*. May 16-20, Fairbanks, Alaska.

Stamnes, K. 1982. Reflection and transmission by vertically inhomogeneous planetary atmosphere, *Planet. Space Sci.*, **30**(7), 727-732.

Ricchiazzi, P., C. Gautier, and D. Lubin. 1995. Cloud scattering optical depth and local surface albedo in the Antarctic: Simultaneous retrieval using ground-based radiometry, *J. Geophys. Res.*, **20**, 21091-21105.